Energy 286 (2024) 129576

Contents lists available at ScienceDirect

Energy

journal homepage: www.elsevier.com/locate/energy

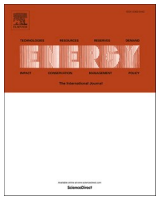

Multi-stage and multi-timescale optimal energy management for hydrogen-based integrated energy systems

Xiaolun Fang [a], Wei Dong [a], Yubin Wang [b], Qiang Yang [b,*]

[a] School of Automation, Hangzhou Dianzi University, Hangzhou, 310018, China
[b] College of Electrical Engineering, Zhejiang University, Hangzhou, 310027, China

ARTICLE INFO

Handling Editor: A. Olabi

Keywords:
Hydrogen
Hydrogen-based integrated energy system
Multi-stage and multi-timescale energy management

ABSTRACT

With the technological advances of flexible multiple energy conversion and utilization, hydrogen energy has attracted increasing attention. The hydrogen-based integrated energy system (HIES) consisting of multiple microgrids (MGs) with hydrogen exchanges among MGs is considered a promising hydrogen utilization paradigm. To facilitate the coordination among multiple MGs, this paper proposed a multi-stage and multi-timescale energy management for a HIES considering the electricity-heat-hydrogen supply-demand balance and demand uncertainties. The proposed solution consists of three stages, i.e. the day-ahead scheduling stage, model predictive control (MPC) based intraday rolling dispatch stage and intraday real-time adjustment stage to participate in the electricity and hydrogen market. In the HIES, hydrogen energy can be dispatched and utilized across MGs to enable flexible energy management and improve energy utilization efficiency. The proposed solution is extensively assessed through the IEEE 33-bus test network with a HIES compared with three benchmark solutions and the numerical results confirm its effectiveness and economic benefits.

1. Introduction

At present, fossil fuels are the main backbone of the global energy system, leading to pollution emissions and energy crises, and hence reducing emissions have become received widespread attention [1–3]. As a zero-carbon fuel, hydrogen energy become an attractive and promising choice for future energy systems [4]. Hydrogen can be produced from a variety of sources, e.g., water, fossil fuels, or biomass, and utilized as an energy source or fuel. Typically, hydrogen can be produced using water electrolyzer (EL) devices, i.e. power-to-hydrogen (P2H) technology [5]. Besides, hydrogen energy can be used to directly supply the hydrogen demand and can generate both electricity and heat through fuel cell-based combined heat and power (FC–CHP) units [6]. Moreover, in the distributed electricity network with a high proportion of renewable energy, hydrogen-based energy systems can absorb the excess renewable energy (e.g. photovoltaic (PV) and wind turbine (TW) systems) and release it when needed. This flexibility allows for better integration and utilization of hydrogen-based energy systems within the distributed electricity network.

In the transportation sector, the widespread use of conventional fossil-fuel-dependent vehicles is one of the main causes of environmental pollution. In addition to plug-in electric vehicles (PEVs), hydrogen fuel vehicles (HFVs) have also emerged as a promising alternative to traditional fossil-fuel-dependent vehicles [7,8]. Against this background, HFVs deployment should be accompanied by the simultaneous establishment of the corresponding infrastructure in the transportation systems. In Ref. [9], an off-grid charging station consisting of solar energy, diesel generation and hydrogen storage for supplying PEVs and HFVs was designed to minimize the investment and operating costs. In Ref. [10], considering the depreciation, fixed cost and hydrogen selling price of the existing stations, a location strategy for new hydrogen fueling stations aiming at maximizing the profit of a new station was proposed. Moreover, several studies focus on the application of hydrogen fueling stations integrated with the electric distribution network considering the power flow constraints. In Ref. [11], the authors placed the charging stations in the selected bus terminals for supplying PEVs and HFVs considering the subsidies without consideration of the dynamics of HFVs demand. In Ref. [12], a supervisory-based model for hydrogen fueling stations was developed to provide both the transportation sector and operating reserve market, and a 33-bus distribution network is used to evaluate this model.

In addition, due to the high energy storage density and long lifetime

* Corresponding author.
E-mail address: qyang@zju.edu.cn (Q. Yang).

https://doi.org/10.1016/j.energy.2023.129576
Received 28 October 2022; Received in revised form 13 August 2023; Accepted 2 November 2023
Available online 4 November 2023

of hydrogen energy storage devices, as well as breakthroughs in hydrogen production, storage and transportation technologies, the research efforts on hydrogen-based energy systems have intensified [13]. Researchers have been actively exploring the integration of hydrogen-based energy systems into existing infrastructure, with a focus on optimizing efficiency, improving storage capabilities, and enhancing overall system performance. This holds great promise for the widespread adoption and utilization of hydrogen as a clean and sustainable energy solution in various sectors. In Ref. [14], considering an electricity-hydrogen flexible conversion process, a long-term optimal planning model and a seasonal hydrogen storage model are proposed for a hybrid energy system. In Ref. [15], combined with electricity, hydrogen and heat storage, a two-layer optimization model was constructed to reduce the annual carbon emissions and costs. Focused on the interaction between wind turbines (WT) and hydrogen storage systems, a distribution network expansion planning solution was presented in Ref. [16] and a stochastic day-ahead scheduling model was developed in Ref. [17] with the consideration of the price-based demand response. In Ref. [18], a day-ahead scheduling model is proposed for an MG with a hydrogen storage system to alleviate the intermittency of renewable energy. In Ref. [19], a risk-averse hybrid solution was proposed for an MG participating in the electricity, gas, thermal and hydrogen markets to increase the entire system's efficiency.

Further, the efficiency of fuel cells i.e. hydrogen-to-power (H2P) technology, is generally between 40 and 60 %. However, if waste heat is captured using FC-CHP devices, e.g., Polymer Electrolyte Membrane Fuel Cells, an efficiency of up to 90 % can be obtained [20]. Due to the high energy efficiency, the FC-CHP has shown great potential for exploiting FC-CHP in MGs to co-supply local electricity and heat demands. In Ref. [21], an system planning problem of an MG with multi-energy storage and FC-CHP units was formulated to minimize annual capital and operation cost. In Ref. [22], the authors proposed a resilience-oriented operation model for an integrated hydrogen-electricity-heat MG with multi-energy storage and FC-CHP units, which aims to improve load survivability. In Ref. [23], for an MG equipped with hydrogen fueling stations, PEVs parking lots and FC-CHP units, a day-ahead scheduling strategy was proposed, which considered the transaction in both hydrogen and electricity markets.

Although many studies have been carried out for energy management in single hydrogen-based MGs (e.g. Refs. [17–19,23]), multiple MGs system get more attention to realize the cooperation among MGs [24]. Moreover, the energy management problem for multi-MGs systems is considered more complex due to the coupling and interactions among MGs [25,26]. However, existing studies exploited the participation of MGs in the electricity and hydrogen market without the consideration of the hydrogen coordination among multiple MGs. Although using pipelines to transport hydrogen is more suitable for long-distance at present, authors in Ref. [27] noted that as the hydrogen market matures, pipelines have a cost advantage in hydrogen energy transportation. Thus hydrogen pipelines would be a desirable option for short-distance transport over a wide area. In this regard, this work focuses on a hydrogen-based integrated energy system (HIES) consisting of multiple MGs, i.e. electricity-hydrogen integrated charging stations (EHI-CS) and industrial MG. Besides, P2H technology is considered in EHI-CS to guarantee the hydrogen demands, and FC-CHP technology is considered in the industrial MG to supply electricity and heat demands. In addition, the HIES actively participates in both the electricity and hydrogen markets. The coordination of hydrogen energy among multiple MGs is considered to enhance the reliability of the system's energy supply. This integrated approach enables efficient management of hydrogen resources and improves overall system performance within the HIES framework.

Our previous work [28] developed an energy management solution for a hydrogen-based MG considering electricity and hydrogen trading among interconnected subsystems in the context of a microgrid. Unlike [26], this work exploits a multi-stage and multi-timescale optimal energy management solution at a power distribution level considering multiple energy forms (i.e. electricity, hydrogen and heat) and multiple energy markets (i.e. electricity market and hydrogen market). The coordination and tight couplings among multi-energy facilities and the hydrogen transaction among MGs enable flexible HIES energy management to accommodate the electricity and hydrogen market. To further improve the energy management strategy, a multi-stage and multi-timescale energy management for the HIES is proposed to minimize the daily HIES operational cost with consideration of electricity-heat-hydrogen supply and demand balance and demand uncertainties. The main contributions of this work are summarized as follows:

(1) This work presented a multi-stage and multi-timescale energy management solution for a HIES to minimize the daily operational cost. Multiple energy forms, timescales and MGs are originally coordinated to establish the electricity-heat-hydrogen supply and demand balance model.
(2) Hydrogen transactions among MGs are fully considered to implement flexible energy management for HIES and participation in the both electricity and hydrogen market.
(3) The proposed solution is extensively evaluated through the IEEE 33-bus test network with a HIES, including three EHI-CSs and an industrial MG, compared against three benchmark solutions, and the numerical results confirm its effectiveness and economic benefits.

The rest of the paper is organized as follows: Section 2 describes the HIES framework and the modeling of controllable units, multi-energy balance and electricity network; Section 3 presents the proposed multi-stage and multi-timescale energy management solution; Section 4 evaluates the proposed solution through an IEEE 33-bus test network connected with a HIES; finally, Section 5 is the conclusive remarks.

2. System model

2.1. HIES description

This paper focuses on a HIES that is composed of a set of MGs (including EHI-CSs and industrial MGs). These MGs are interconnected through both the electricity network and the hydrogen network, and are supervised by a HIES aggregator, as depicted in Fig. 1(a). In the electricity network system, apart from HIES, a considerable proportion of renewable energy sources, e.g., PVs and WTs, are integrated. In the HIES, MGs can purchase energy from electricity and hydrogen markets and hydrogen pipelines are available among MGs for hydrogen exchange. To facilitate the HIES energy management, the local controller (LC) in the MG needs to measure and forecast the demand and make them available to the HIES aggregator [29]. Then, the coordinated energy scheduling and dispatch of the HIES can be carried out through optimization in the HIES aggregator considering demand uncertainty and network constraints.

The EHI-CS and industrial MG are illustrated in Fig. 1 (b) and (c), respectively. The former mainly consists of hydrogen production and storage equipment (i.e. EL and hydrogen tanks), battery energy storage system (BESS) and electricity and hydrogen demand (i.e. PEVs and HFVs). The latter consists of an FC-CHP unit (including fuel cell and heat exchanger), EB, heat energy tanks, BESS and electricity and heat demand. The FC-CHP unit can meet both electrical and thermal demands using hydrogen and atmospheric oxygen. In addition to FC-CHP, heat demands can also be met by EB units, and residual heat can be stored in heat storage tanks.

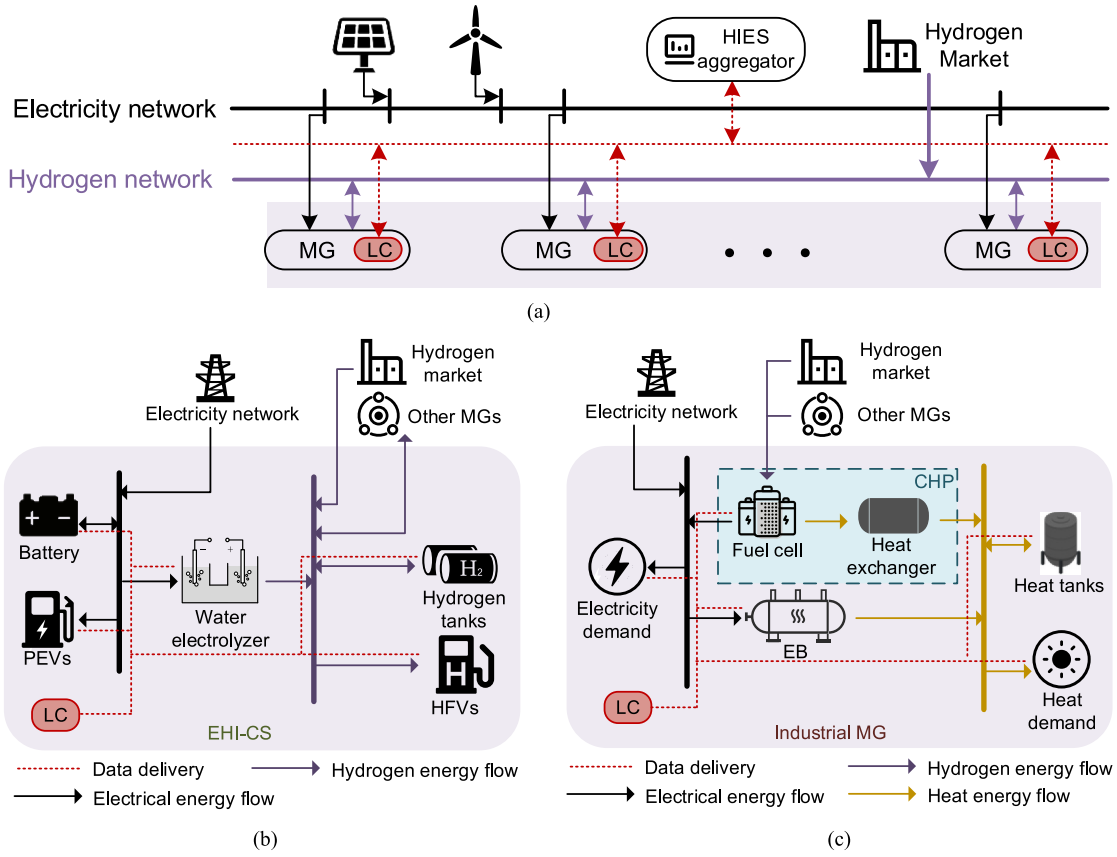

Fig. 1. Operation framework for (a) network with multiple MGs; (b) EHI-CS for PEVs and HFVs; and (c) industrial MG.

2.2. Modeling of controllable units in MG

2.2.1. EL unit

Energy conversion of the EL is modeled by Eq. (1), and Eq. (2) denotes the limit bounds of hydrogen generated by the EL.

$$H_m^{\mathrm{EL}}(t) = P_m^{\mathrm{P2H}}(t) E^{\mathrm{P2H}} \eta^{\mathrm{EL}} \tag{1}$$

$$P_{\min}^{\mathrm{P2H}} \le P_m^{\mathrm{P2H}}(t) \le P_{\max}^{\mathrm{P2H}} \tag{2}$$

where t is the time slot index; H_m^{EL} and P_m^{P2H} are the hydrogen production and electricity consumption of the EL in the mth MG, respectively; E^{P2H} is the P2H conversion factor; η^{EL} is the efficiency of the EL; $P_{\min}^{\mathrm{P2H}}$ and $P_{\max}^{\mathrm{P2H}}$ are maximum and minimum input electric power of the EL, respectively.

2.2.2. Hydrogen storage unit

The hourly stored hydrogen for the hydrogen storage tank is given by (3), and the tank's capacity and the power charging/discharging rate are limited as Eqs. (4) and (5), respectively.

$$HS_m(t) = HS_m(t-1) + H_m^{\mathrm{EL}}(t) - H_m^{\mathrm{HFV}}(t) + H_{\mathrm{all},m}^{\mathrm{buy}}(t) - H_{\mathrm{all},m}^{\mathrm{sell}}(t) \tag{3}$$

$$HS_{\min} \le HS_m(t) \le HS_{\max} \tag{4}$$

$$-H_{\max}^{\mathrm{ch}} \le HS_m(t) - HS_m(t-1) \le H_{\max}^{\mathrm{ch}} \tag{5}$$

where HS_m is the stored hydrogen in the hydrogen tank; H_m^{HFV} represents the HFV demands; $H_{\mathrm{all},m}^{\mathrm{buy}}$ and $H_{\mathrm{all},m}^{\mathrm{sell}}$ denote total hydrogen purchased/sold for the mth MG; $HS_{\max}$ and $HS_{\min}$ are the maximum and minimum value of hydrogen storage; $H_{\max}^{\mathrm{ch}}$ is the maximum hydrogen charging and discharging limit for the hydrogen tank.

2.2.3. BESS unit

The state of charge (SOC) of the BESS at each time slot can be expressed as Eq. (6), and the SOC should be within a certain range, which can be described as Eq. (7). As described in Eq. (8), two binary variables $I_m^{\mathrm{Bat,ch}}$ and $I_m^{\mathrm{Bat,disc}}$ are introduced to ensure that the battery cannot charge and discharge simultaneously, and charging and discharging power of the battery are limited in Eqs. (9) and (10).

$$SOC_m(t) = SOC_m(t-1) + \frac{\left(P_m^{\mathrm{Bat,ch}}(t)\eta^{\mathrm{ch}} - P_m^{\mathrm{Bat,disc}}(t)/\eta^{\mathrm{disc}}\right)}{C_m^{\mathrm{Bat}}}\Delta t \tag{6}$$

$$SOC_{\min} \le SOC_m(t) \le SOC_{\max} \tag{7}$$

$$I_m^{\mathrm{Bat,ch}}(t) + I_m^{\mathrm{Bat,disc}}(t) \le 1 \tag{8}$$

$$0 \le P_m^{\mathrm{Bat,ch}}(t) \le P_{\max}^{\mathrm{Bat,ch}} I_m^{\mathrm{Bat,ch}}(t) \tag{9}$$

$$0 \le P_m^{\mathrm{Bat,disc}}(t) \le P_{\max}^{\mathrm{Bat,disc}} I_m^{\mathrm{Bat,disc}}(t) \tag{10}$$

where SOC_m denotes the state of capacity of the battery; $P_m^{\mathrm{Bat,ch}}$ and $P_m^{\mathrm{Bat,disc}}$ denote the charging and discharging power of the battery. η^{ch} and η^{disc} are the efficiency of battery charging and discharging. C^{Bat} denotes the capacity of the battery; $SOC_{\min}$ and $SOC_{\max}$ are the SOC upper and lower limit, and $P_{\max}^{\mathrm{Bat,ch}}$ is the maximum power charging/discharging rate.

2.2.4. FC-CHP unit

The FC-CHP consists of fuel cells and a heat exchanger. Fuel cells consumed hydrogen to generate electricity while the remaining generated heat is targeted for recovery through a heat exchanger. The energy conversion of the FC-CHP can be expressed by Eqs. (11) and (12), and the generated electricity should be limited by Eq. (13)

$$P^{\mathrm{CHP}}(t) = H^{\mathrm{CHP}}(t) E^{\mathrm{H2P}} r^{\mathrm{H2P}} \tag{11}$$

$$G^{\mathrm{CHP}}(t) = P^{\mathrm{CHP}}(t) / d \tag{12}$$

$$0 \le P^{\mathrm{CHP}}(t) \le P^{\mathrm{CHP}}_{\max} \tag{13}$$

where P^{CHP}, G^{CHP} and H^{CHP} denote electricity and heat production, and hydrogen consumption of the FC-CHP. E^{H2P} represent the H2P conversion factor; r^{H2P} and d represent the hydrogen-to-electricity and heat-to-electric ratio of the FC-CHP, respectively; and $P^{\mathrm{CHP}}_{\max}$ denotes the maximum electricity generated by the FC-CHP.

2.2.5. EB unit

The EB can generate heat by using electricity to meet part of the heat demand and its energy conversion and the heat power generated bounds are given in Eq. (14) and Eq. (15), respectively.

$$G^{\mathrm{EB}}(t) = P^{\mathrm{EB}}(t) \eta^{\mathrm{EB}} \tag{14}$$

$$0 \le G^{\mathrm{EB}}(t) \le G^{\mathrm{EB}}_{\max} \tag{15}$$

where G^{EB} and P^{EB} denote heat production and electricity consumption of the EB; η^{EB} is the efficiency of the EB; and $G^{\mathrm{EB}}_{\max}$ is maximum heat power generated by the EB.

2.2.6. Heat storage unit

The stored heat power for the heat storage tank is given by Eq. (16) and the amount of stored heat energy and heat charging/discharging rate need to satisfy Eqs. (17) and (18), respectively.

$$GS(t) = GS(t-1) + G^{\mathrm{ch}}(t) - G^{\mathrm{dis}}(t) \tag{16}$$

$$GS_{\min} \le GS(t) \le GS_{\max} \tag{17}$$

$$-G^{\mathrm{ch}}_{\max} \le GS(t) - GS(t-1) \le G^{\mathrm{ch}}_{\max} \tag{18}$$

where GS denotes the stored heat power; G^{ch} and G^{dis} are charging and discharging heat of the heat tanks; $GS_{\max}$ and $GS_{\min}$ represent the maximum and minimum value of heat power storage, respectively; $G^{\mathrm{ch}}_{\max}$ denotes the maximum charging and discharging heat limit of heat tanks.

2.3. Modeling of multi-energy supply-demand balance

2.3.1. Electricity power balance

The mth MG including each EHI-CS and the industrial MG in each time slot is defined as Eqs. (19) and (20), respectively. Eq. (21) is used to ensure that the electricity power purchased cannot exceed the limitation.

$$P^{\mathrm{PEV}}_m(t) + P^{\mathrm{P2H}}_m(t) + P^{\mathrm{Bat,ch}}_m(t) - P^{\mathrm{Bat,disc}}_m(t) = P^{\mathrm{buy}}_m(t) \tag{19}$$

$$P^{\mathrm{Load}}(t) + P^{\mathrm{EB}}(t) - P^{\mathrm{CHP}}(t) + P^{\mathrm{Bat,ch}}_m(t) - P^{\mathrm{Bat,disc}}_m(t) = P^{\mathrm{buy}}_m(t) \tag{20}$$

$$0 \le P^{\mathrm{buy}}_m(t) \le f_m \tag{21}$$

where P^{PEV}_m and P^{Load} represent the PEV demands and industrial electricity demands; P^{buy}_m is electrical power purchased with the electricity power network; f_m represents the maximum amount of electricity that can purchase from the utility grid.

2.3.2. Hydrogen supply-demand balance

In the EHI-CS, hydrogen supply-demand balance can be denoted by Eq. (3). While in the industrial MG, hydrogen purchased is used for FC-CHP to generate electricity and heat, and described as Eq. (22).

$$H^{\mathrm{CHP}}(t) = H^{\mathrm{buy}}_{\mathrm{all},m}(t) \tag{22}$$

The hydrogen transportation balance in the mth MG is given in Eqs. (23) and (24).

$$H^{\mathrm{buy}}_{\mathrm{all},m}(t) = H^{\mathrm{buy}}_{\mathrm{HM},m}(t) + H^{\mathrm{buy}}_{\mathrm{MG},m}(t) \tag{23}$$

$$H^{\mathrm{sell}}_{\mathrm{all},m}(t) = H^{\mathrm{sell}}_{\mathrm{MG},m}(t) \tag{24}$$

where $H^{\mathrm{buy}}_{\mathrm{HM},m}$ and $H^{\mathrm{buy}}_{\mathrm{MG},m}$ denote hydrogen purchased from the hydrogen market and other MGs; $H^{\mathrm{sell}}_{\mathrm{MG},m}$ denotes hydrogen sold to other MGs. It should be noted that this paper assumes MG cannot sell hydrogen to the hydrogen market.

Two binary variables $I^{\mathrm{H,buy}}_m$ and $I^{\mathrm{H,sell}}_m$ are used here to ensure that the MG does not purchase and sell hydrogen simultaneously, as given in Eq. (25). Hydrogen power purchased/sold by each MG is limited in Eq. (26) and Eq. (27).

$$I^{\mathrm{H,buy}}_m(t) + I^{\mathrm{H,sell}}_m(t) \le 1 \tag{25}$$

$$0 \le H^{\mathrm{buy}}_{\mathrm{all},m}(t) \le H^{\mathrm{trans}}_{\max} \times I^{\mathrm{H,buy}}_m(t) \tag{26}$$

$$0 \le H^{\mathrm{sell}}_{\mathrm{sll},m}(t) \le H^{\mathrm{trans}}_{\max} \times I^{\mathrm{H,sell}}_m(t) \tag{27}$$

where $H^{\mathrm{trans}}_{\max}$ denotes the maximum hydrogen transportation.

2.3.3. Heat supply-demand balance

The heat power balance constraint of the industrial MG can be modeled as Eq. (28).

$$G^{\mathrm{EB}}(t) + G^{\mathrm{CHP}}(t) + G^{\mathrm{dis}}(t) = G^{\mathrm{Load}}(t) + G^{\mathrm{ch}}(t) \tag{28}$$

where G^{Load}_m is the heat demand in the industrial MG.

2.4. Modeling of electricity network

The electricity network power flow model is formulated with the branch-flow mode (BFM), which is widely used in distribution systems [29] and is represented by Eqs. (29)–(32). The bus voltage and branch current are limited by Eqs. (33) and (34).

$$\left|V_j(t)\right|^2 = \left|V_i(t)\right|^2 - 2\left(r_{ij}P_{ij}(t) + x_{ij}Q_{ij}(t)\right) + \left(r_{ij}^2 + x_{ij}^2\right)\left|I_{ij}(t)\right|^2 \tag{29}$$

$$q_j(t) = Q_{ij}(t) - x_{ij}\left|I_{ij}(t)\right|^2 - \sum_{k:j\to k} Q_{jk}(t) \tag{30}$$

$$p_j(t) = P_{ij}(t) - r_{ij}\left|I_{ij}(t)\right|^2 - \sum_{k:j\to k} P_{jk}(t) \tag{31}$$

$$\left|V_i(t)\right|^2 \times \left|I_{ij}(t)\right|^2 \le P_{ij}^2(t) + Q_{ij}^2(t) \tag{32}$$

$$\left|V_{\min}\right|^2 \le \left|V_i(t)\right|^2 \le \left|V_{\max}\right|^2 \tag{33}$$

$$0 \le \left|I_{ij}(t)\right|^2 \le \left|I_{\max}\right|^2 \tag{34}$$

where i and j is the bus index; ij denotes the branch ij (bus i to bus j); $|V_i(t)|$ is the voltage magnitude; $|I_{ij}(t)|$ is the current magnitude; r_{ij} and x_{ij} are resistance and reactance; P_{ij} and Q_{ij} are the active and reactive power flows; q_j and p_j are the active the reactive power injection; $V_{\max}$ and $I_{\max}$ are the maximum magnitude of the bus voltage and branch current. Moreover, for the node with renewable energy (e.g., PV or WT), the active and reactive power injections are represented by Eqs. (35) and (36).

$$p_j(t) = P_j^{Load}(t) - P_j^{REN}(t) \tag{35}$$

$$q_j(t) = Q_j^{Load}(t) - Q_j^{REN}(t) \tag{36}$$

where P_j^{Load} and P_j^{REN} denote active power load and electrical power generation of renewable energy (e.g., PV and WT); Q_j^{Load} and Q_j^{REN} denote reactive power load and reactive power generation of reactive devices (e.g., static var compensator(SVC)) connected to bus j [30]. Renewable energy power generation is limited by Eq. (37).

$$0 \le P_j^{REN}(t) \le P_{j,\max}^{REN}(t) \tag{37}$$

where $P_{j,\max}^{REN}$ represents the maximum power generation of the renewable energy system.

3. Problem formulation

Fig. 2 illustrates the proposed multi-stage energy management solution for the HIES. As the hydrogen and heat demands are generally scheduled at the hourly timescale and the electrical energy fluctuates on the minute timescale, the energy management for the multi-energy HIES is considered a multi-timescale optimization problem [31]. Thus, due to the different dispatch timescales of multiple forms of energy, real-time dispatch optimization can be divided into slow time scale (STS) and fast time scale (FTS) problems. The relationship between STS and FTS is described in Eq. (38), where t_s and t_f denote the time slot index of STS and FTS, and z denotes the time slot number of FTS in each time interval of STS. It can be interpreted as the FTS time slot t_f ($t_f \in [z(t_s-1)+1, zt_s]$) belonging to the STS time slot t_s [32].

$$z = \Delta t_s / \Delta t_f \tag{38}$$

As shown in Fig. 2 (a), the proposed solution consists of three different stages, i.e. the day-ahead scheduling stage, intraday rolling dispatch stage and intraday real-time adjustment stage, described as follows.

(1) Day-ahead scheduling stage: according to the day-ahead electricity price and day-ahead demand prediction data, the HIES aggregator performs day-ahead scheduling to determine electricity procurement for each MG with a timescale of 1 h.
(2) Intraday rolling dispatch stage: based on the intraday electricity market and short-term demand prediction, the HIES aggregator carries out an MPC-based rolling dispatch with a timescale of 1 h to reduce the negative effect of the day-ahead prediction error. As shown in Fig. 2(b), in this work, the rolling horizon is considered as 4 h with the calculated results for the first 1 h being implemented, and after finishing a real-time dispatch decision, the rolling horizon moves forward by a one-time slot.
(3) Intraday real-time adjustment stage: based on the intraday electricity market and electricity demand in the current slot, the HIES aggregator executes a real-time adjustment optimization for the electricity with a timescale of 15 min s.

It should be highlighted that, unlike the solution proposed in Ref. [28] that the electricity dispatch was carried out based on short-term demand prediction and rolling optimization over multiple time slots, this work only requires optimization for one time slot based on the current renewable power generation (i.e. WT and PV) and demand. Hence, the computational complexity of real-time electricity dispatch can be significantly reduced and the efficiency of energy management is improved.

3.1. Day-ahead scheduling model

3.1.1. Objective function

According to the day-ahead clearing price and the electricity, hydrogen and heat demand prediction in individual MGs, the HIES aggregator makes its economic optimization plan to minimize the total

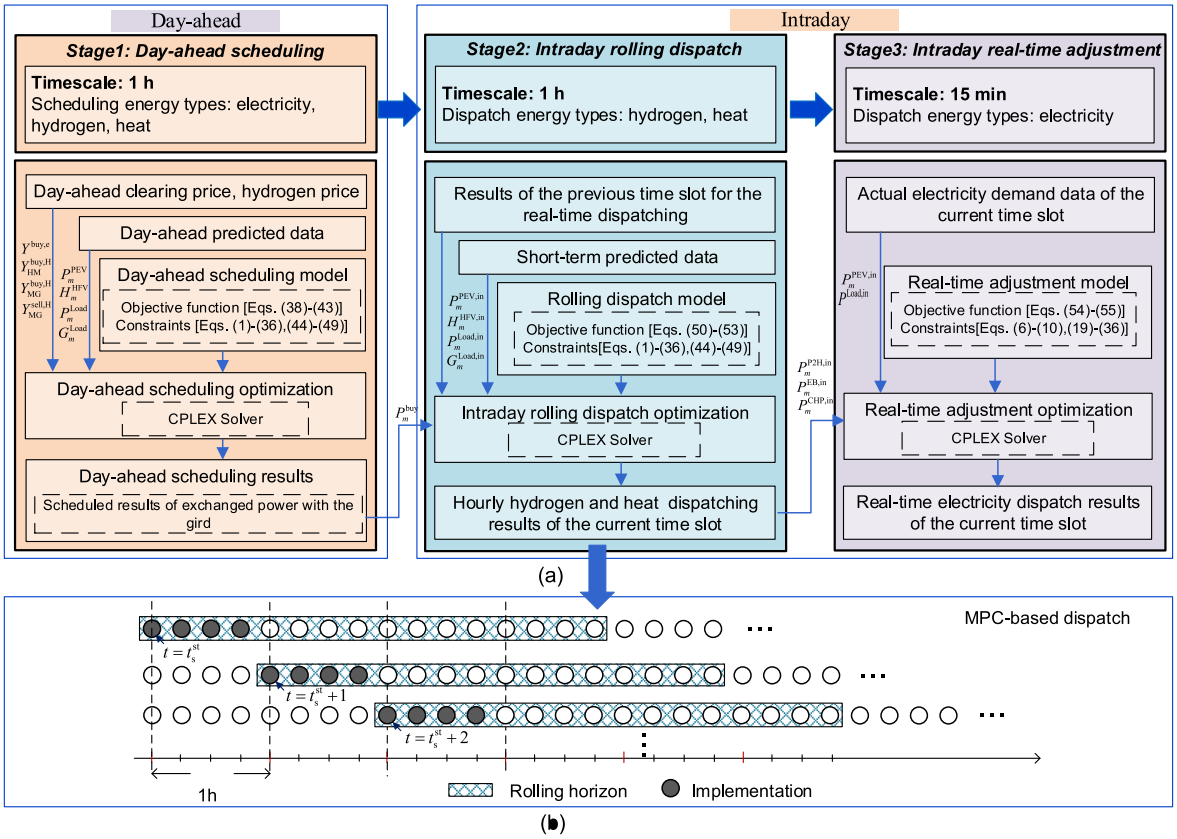

Fig. 2. Framework of the proposed multi-stage energy management solution includes: (a) flowchart of the energy management algorithm; and (b) MPC-based intraday rolling dispatch.

daily operation cost, and the objective function is modeled by Eqs.(39)–(44). The objective function is represented in Eq. (39) which minimizes the total cost due to electricity and hydrogen transactions and the device cost. Eq. (40) denotes the total cost of electricity transactions. Eq. (41) denotes the cost of hydrogen power transactions with the hydrogen market and among MGs. Eqs. (42) and (43) are cost functions of the P2H unit and the FC-CHP unit, respectively. The first term is unit operation and maintenance costs, related to working hours, and the second is the degradation cost, which is mainly related to their start-up and shut-down times [33,34]. Eq. (44) denotes the daily cost of batteries, including the cycling cost and the degradation cost [35].

$$\min OF = \sum_{t_s=1}^{T_s} \left(F^{e}(t_s) + F^{H}(t_s) + F^{P2H}(t_s) + F^{CHP}(t_s) + F^{BESS}(t_s)\right)\Delta t_s \tag{39}$$

$$F^{e}(t_s) = \sum_{m=1}^{M} Y^{buy,e}(t_s) P_m^{buy}(t_s) \tag{40}$$

$$F^{H}(t_s) = \sum_{m=1}^{M} \left(Y_{HM}^{buy,H}(t_s) H_{HM,m}^{buy}(t_s) + Y_{MG}^{buy,H}(t_s) H_{MG,m}^{buy}(t_s) - Y_{MG}^{sell,H}(t_s) H_{MG,m}^{sell}(t_s)\right) \tag{41}$$

$$F^{P2H}(t_s) = \sum_{m=1}^{M} \left(\left(\frac{CC^{EL}}{Hours^{EL}} + c^{EL}\right) I_m^{P2H}(t_s) + e^{EL}\left(\sigma_m^{EL,on} + \sigma_m^{EL,off}\right)\right) \tag{42}$$

$$F^{CHP}(t_s) = \left(\frac{CC^{CHP}}{Hours^{CHP}} + c^{CHP}\right) I^{CHP}(t_s) + e^{CHP}\left(\sigma^{CHP,on} + \sigma^{CHP,off}\right) \tag{43}$$

$$F^{Bat}(t_s) = \sum_{m=1}^{M} \left(\begin{array}{l} \dfrac{CC^{Bat}}{2Cycles^{Bat}} P_m^{Bat,ch}(t_s)\eta^{ch} + \dfrac{CC^{Bat}}{2Cycles^{Bat}\eta^{disc}} P_m^{Bat,disc}(t_s) \\ +\rho_b a_n \left((\Delta SOC_m(t_s))^{\beta_k} + \eta_n\right)^{-1} SOH_m(t_s) \end{array} \right) \tag{44}$$

where $Y^{buy,e}$ is the day-ahead electricity purchasing price; $Y_{HM}^{buy,H}$ is the hydrogen price in the hydrogen market; $Y_{MG}^{buy,H}$ and $Y_{MG}^{sell,H}$ are the price of buying/selling hydrogen among MGs; CC^{EL} and CC^{CHP} denote the capital cost for the EL and CHP units; $Hours^{EL}$ and $Hours^{CHP}$ denote the number of life hours; c^{EL} and c^{CHP} are the O&M cost function coefficients; e^{EL} and e^{CHP} are the start-up and shutdown cost function coefficients; $\sigma_m^{EL,on}$ and $\sigma^{CHP,on}$ represent the start-up times; $\sigma_m^{EL,off}$ and $\sigma^{CHP,off}$ represent the shutdown times; and I_m^{P2H} and I^{CHP} are the binary status indicators of the EL and CHP units. $CC^{bat\#k}$ and $Cycles^{Bat}$ are the capital cost and the life cycle of the battery, respectively; ρ_b a_n β_k η_n are degradation parameters for BESS. SOH_m denotes the BESS state of health, which is normalized to the interval [0, 1].

3.1.2. Constraints

In the day-ahead scheduling model, energy device constraints should be met: EL constraints Eqs. (1) and (2), hydrogen storage constraints Eqs. (3)–(5), BESS constraints Eqs. (6)–(10), FC-CHP constraints Eqs. (11)–(13), EB constraints Eqs.(14) and (15), and heat storage constraints Eqs.(16)–(18). Moreover, the constraints Eq.(45)–(50) for BESS, hydrogen and heat storage system need to be met to ensure the same flexible scheduling on every scheduling day.

$$SOC_m(0) = SOC_{ini} \tag{45}$$

$$SOC_m(T_s) = SOC(0) \tag{46}$$

$$HS_m(0) = HS_{m,ini} \tag{47}$$

$$HS_m(T_s) = HS_m(0) \tag{48}$$

$$GS(0) = GS_{ini} \tag{49}$$

$$GS(T_s) = GS(0) \tag{50}$$

where SOC_{ini}, $HS_{m,ini}$ and GS_{ini} are the initial electricity, hydrogen and heat storage values, respectively. In addition, Multi-energy supply and demand balance for electricity, hydrogen and heat constraints Eqs.(19)–(28) and electricity network constraints Eqs. (29)–(36) should be satisfied.

3.2. Intraday rolling dispatch model

3.2.1. Real-time market

The intraday electricity dispatch is aiming to minimize the penalty cost due to real-time market (RTM) participation, which is based on a dual-pricing market [36]. In detail, in intraday trading with the utility grid, electricity consumption below or over the schedule will be fined. Thus, the inevitable deviations between prediction and real-time actual demand may lead to a distinct additional penalty for the power imbalance.

3.2.2. Objective function

Based on the day-ahead scheduled results and the intraday short-term demand prediction, the MPC-based rolling dispatch is carried out. In the intraday rolling dispatch model, the objective function is illustrated in Eq. (51) which minimizes the penalty cost, hydrogen transaction cost and actual device operating cost. The penalty cost of electricity power imbalance is modeled as Eqs.(52)–(54). It should be noted that hydrogen trading and a collection of controllable facilities in the HIES can be managed to coordinate day-ahead scheduling and real-time dispatch Hence, the terms associated with the cost of hydrogen transaction ($F^{H,RTM}$) and the cost of EL ($F_t^{P2H,RTM}$), CHP ($F_t^{CHP,RTM}$) and BESS ($F^{BESS,RTM}$) cannot be ignored, and their expressions are similar to Eqs. (41)–(44).

$$\begin{aligned} \min OF^{ROLL} = \sum_{t_s=t_s^{st}}^{T_s} \big(&F^{e,RTM}(t_s) + F^{H,RTM}(t_s) + F^{P2H,RTM}(t_s) + F^{CHP,RTM}(t_s) \\ &+ F^{BESS,RTM}(t_s)\big)\Delta t_s \end{aligned} \tag{51}$$

$$F^{e,RTM}(t_s) = \sum_{m=1}^{M} \sum_{t_f \in t_s} C_m^{im}(t_f) \tag{52}$$

$$C_{grid,m}^{im}(t_f) = \begin{cases} Y^{im,below}\left(\lceil t_f/z \rceil\right) \times P_m^{im}(t_f), P_m^{im}(t_f) \le 0 \\ Y^{im,excess}\left(\lceil t_f/z \rceil\right) \times P_m^{im}(t_f), P_m^{im}(t_f) \ge 0 \end{cases} \tag{53}$$

$$P_m^{im}(t_f) = P_m^{buy,in}(t_f) - P_m^{buy}\left(\lceil t_f / z \rceil\right) \tag{54}$$

where, the superscripts "RTM" and "in" denote the variables of the RTM participation and the values in the intraday rolling dispatch model, respectively. The function " $\lceil \cdot \rceil$" is used to round up to the smallest integer not less than the variable. $Y^{im,below}$ and $Y^{im,excess}$ are the negative and positive imbalance price; P_m^{im} is the imbalance power.

3.2.3. Constraints

Similar to the day-ahead scheduling model, in the intraday rolling dispatch stage, the operational constraints of each component (i.e. Eqs. (1)–(18), (47)–(50)) multi-energy supply-demand balance constraints (i.e. Eqs.(19)–(28)) and electricity network constraints (i.e. Eqs.(29)–(36)) should be satisfied.

3.3. Intraday real-time adjustment model

3.3.1. Objective function

In the third level, based on the actual electricity demand of the current time slot and the hourly hydrogen/heat energy dispatch results,

only the electricity part participates in real-time optimization to realize the real-time adjustment. In this stage, the objective function in the time slot t_f is given in Eq. (55) including the penalty cost and the BESS cost. The penalty cost of electricity energy imbalance in the time slot t_f is given in Eq. (56) and BESS cost $F^{\mathrm{BESS,ADJ}}$ is similar to Eq. (44)

$$\min OF^{ADJ} = \left(F^{\mathrm{e,ADJ}}\left(t_f\right) + F^{\mathrm{BESS,ADJ}}\left(t_f\right)\right)\Delta t_f \tag{55}$$

$$F^{\mathrm{e,ADJ}}\left(t_f\right) = \sum_{m=1}^{M} C^{\mathrm{im}}_{\mathrm{grid},m}\left(t_f\right) \tag{56}$$

where, the superscripts "ADJ" represents the variables in the intraday real-time adjustment model.

3.3.2. Constraints

In this stage, the BESS operational constraints (i.e. Eqs. (6)–(10)), electricity supply-demand balance constraints (i.e. Eqs.(19)–(28)), and electricity network constraints (i.e. Eqs.(29)–(36)) should be satisfied.

4. Simulations and numerical results

4.1. Simulation setup

In this work, the IEEE 33-bus test network [37] with 4 MGs (including three EHI-CSs and an industrial MG) is adopted for assessment of the proposed HIES multi-stage and multi-timescale energy management solution, as illustrated in Fig. 3. In this test electricity network, three PV generation systems are connected in bus 15, 24 and 32 with rated capacities of 1.2 MW, 2.2 MW, and 1.4 MW respectively. One WT generation system is connected to bus 21 with a rated capacity of 2.6 MW. Here, the positive and negative imbalance price is 2/0.8 times the day-ahead electricity price, i.e. $Y^{\mathrm{im,excess}}(t) = 2Y^{\mathrm{buy,e}}(t)$ and $Y^{\mathrm{im,below}}(t) = 0.8Y^{\mathrm{buy,e}}(t)$, respectively [38], and the day-ahead electricity purchasing price used in this test study is illustrated in Fig. 4(a) from ISO New England history data [39]. Moreover, it is assumed that the hydrogen selling price is 0.95 times of purchasing price among MGs, which is lower than the hydrogen purchase price from the hydrogen market, i.e. $Y^{\mathrm{sell,H}}_{\mathrm{MG}} = 0.95Y^{\mathrm{buy,H}}_{\mathrm{MG}}$, $Y^{\mathrm{buy,H}}_{\mathrm{MG}} = 2.4$ \$/kg, and $Y^{\mathrm{buy,H}}_{\mathrm{HM}} = 4$ \$/kg [40].

In the test system, the modeling parameters for components in the HIES are listed in Table 1 [34,41], and simulating parameter $f_m = 1.6$ MW, $V_{\max}/V_{\min} = 1.05/0.95$. To leave some intraday dispatch space for the HIES, the following parameter values are chosen in the day-ahead scheduling optimization: $P^{\mathrm{P2H}}_{\max} = 0.8$ MW, $HS_{\max}/HS_{\min} = 240/36$ kg, $H^{\mathrm{ch}}_{\max} = 80$ kg, $P^{\mathrm{CHP}}_{\max} = 1.6$ MW, $G^{\mathrm{EB}}_{\max} = 0.32$ MW, $GS_{\max}/GS_{\min} = 2.4/0.12$ MW, $G^{\mathrm{ch}}_{\max} = 0.8$ WM and $f_L = 1.28$ MW [42]. Similarly, the value of f_L in the intraday rolling dispatch stage is set as 1.44 MW. Moreover, the day-ahead predicted data and the actual data for electricity, hydrogen and heat demands used in this test study are illustrated in Fig. 4(b)–(e), which are extracted from and [43–46]. Further, according to Ref. [47], it is assumed that the short-term predicted data (4 h) is close to the actual value, and thus, in this work, real data is used for the rolling horizon.

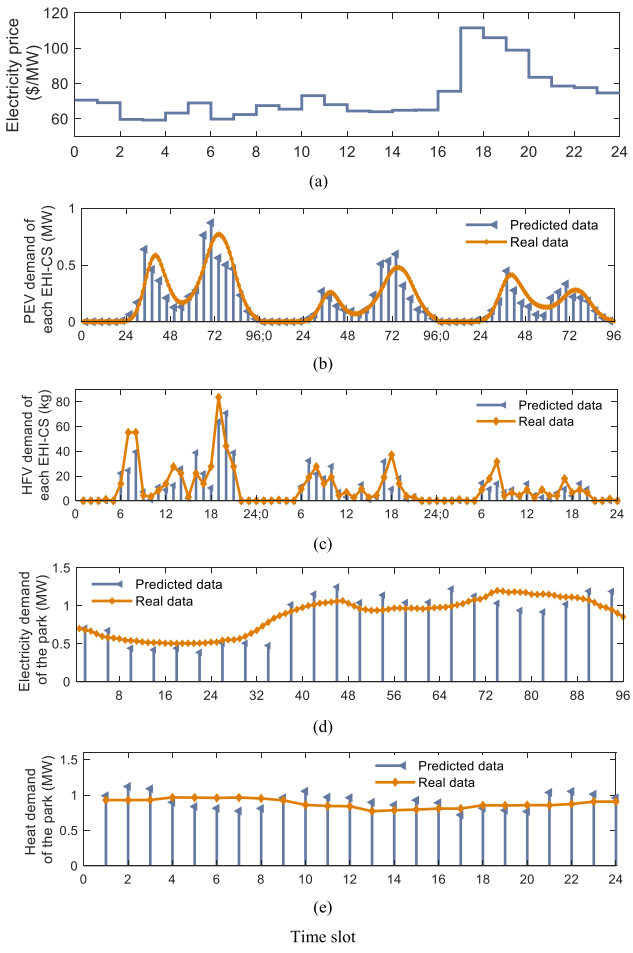

Fig. 4. (a) Day-ahead electric purchasing price; predicted and real data for (b) PEV demands and (c) HFV demand in each EHI-CS; (d) electricity demand; and (e) heat demand on the industrial MG.

All simulations are implemented using MATLAB (version 2018a) and executed on a computer equipped with a 3.20 GHz AMD Ryzen 7 6800HS CPU and 16.00 G RAM. The executive time for decision-making of the day-ahead scheduling is 11.85 s, and the average execution time for one one-time slot decision-making of intraday rolling dispatch and intraday real-time adjustment is 4.17s and 0.58s, respectively.

4.2. Simulation results

Fig. 5 and Fig. 6 show the day-ahead scheduled and intraday dispatch results for hydrogen energy balance on the test day,

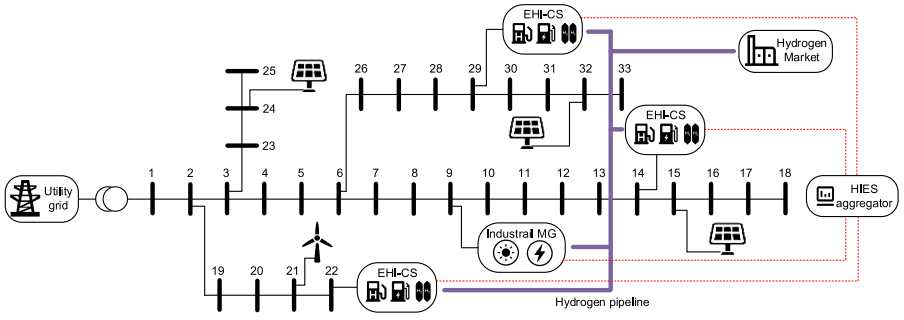

Fig. 3. Schematic of 33-bus test system integrated with multiple MGs under renewable energy penetration.

Table 1
Modeling parameters for components.

EL unit
$P^{\mathrm{P2H}}_{\max}/P^{\mathrm{P2H}}_{\min} = 1.0/0.1MW$, $E^{\mathrm{P2H}} = 0.0254kg/kWh$, $\eta^{\mathrm{EL}} = 0.8$, $CC^{\mathrm{EL}} = 1.25 \times 10^5\$$, $Hours^{\mathrm{EL}} = 50000h$, $c^{\mathrm{EL}} = 0.07\$/h$, $e^{\mathrm{EL}} = 0.38\$$

FC-CHP
$P^{\mathrm{CHP}}_{\max}/P^{\mathrm{CHP}}_{\min} = 2.0/0.2MW$, $E^{\mathrm{H2P}} = 39.4kWh/kg$, $r^{\mathrm{H2P}} = 0.36$, $d = 0.7$, $CC^{\mathrm{CHP}} = 2.0 \times 10^5\$$, $Hours^{\mathrm{CHP}} = 20000h$, $c^{\mathrm{CHP}} = 0.1\$/h$, $e^{\mathrm{CHP}} = 0.1\$$

BESS
$C^{\mathrm{Bat}}_m = 2.0MW$, $SOC_{\max}/SOC_{\min} = 0.8/0.2$, $P^{\mathrm{Bat,ch}}_{\max}/P^{\mathrm{Bat,disc}}_{\max} = 1.0/1.0MW$, $\eta^{\mathrm{ch}}/\eta^{\mathrm{disc}} = 0.9/0.95$, $CC^{\mathrm{Bat}} = 100\$/kWh$, $Cycles^{\mathrm{Bat}} = 3000$, $\rho_b = 100$, $a_n = 0.01$, $\beta_k = -2$, $\eta_n = 0$

Hydrogen storage unit
$HS_{\max}/HS_{\min} = 300/30kg$, $H^{\mathrm{ch}}_{\max} = 100kg$,

Heat storage unit
$GS_{\max}/GS_{\min} = 3.0/0.3MW$, $G^{\mathrm{ch}}_{\max} = 1.0WM$

EB unit
$G^{\mathrm{EB}}_{\max} = 0.6MW$, $\eta^{\mathrm{EB}} = 0.95$

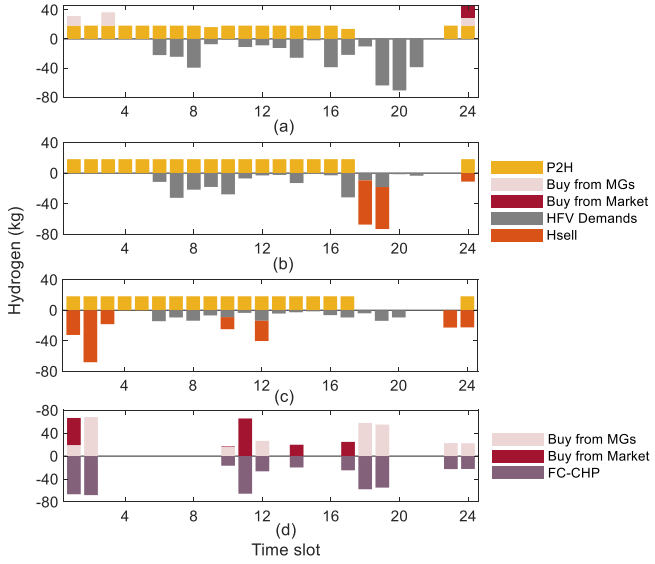

Fig. 5. HIES hydrogen energy balance by the day-ahead scheduled for (a) EHI-CS 1; (b) EHI-CS 2; (c) EHI-CS 3; and (d) industrial MG.

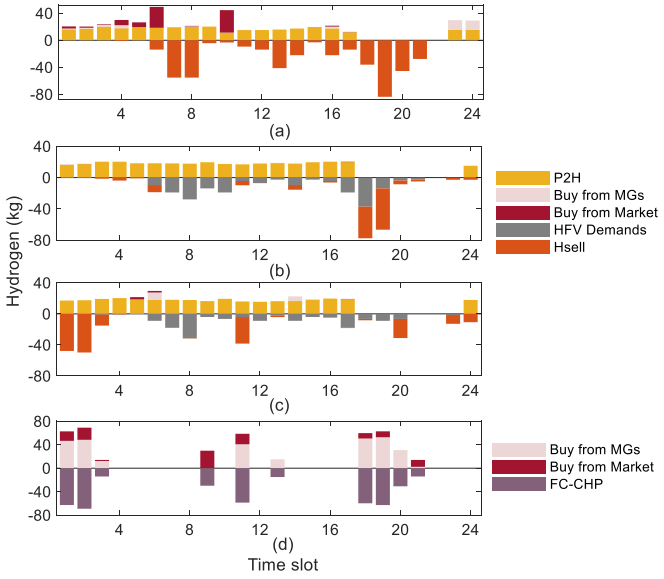

Fig. 6. HIES hydrogen energy balance by the intraday real-time dispatch for (a) EHI-CS 1; (b) EHI-CS 2; (c) EHI-CS 3; and (d) industrial MG.

respectively. Positive values in the figures are the amount of hydrogen obtained that the MGs, i.e. the hydrogen produced from P2H technology and hydrogen purchased from other MGs or the hydrogen market. While negative values present the amount of hydrogen consumed in MGs, i.e. FHV demands and hydrogen sold to other MGs. In EHI-CSs, the difference between positive and negative values can indicate hydrogen storage status. When the positive value is larger than the negative value, the hydrogen storage charge; else, the hydrogen storage discharge. It can be found that in the industrial MG, the positive value is equal to the negative value, i.e. all purchased hydrogen is used in the FC-CHP unit to generate heat and electricity energy. Day-ahead scheduled and intraday actual stored hydrogen results are given in Fig. 7 (a)-(c) and (d)-(f), respectively.

Heat energy balance in the industrial MG by the day-ahead scheduled and intraday actual operation results are illustrated in Fig. 8 and Fig. 9, respectively. In the industrial MG, both FC-CHP and EB can produce heat energy to supply the demands, and the extra heat can be stored in the heat storage tanks. The stored heat by the day-ahead scheduled and intraday actual operation results are shown in Fig. 10 (a) and (b), respectively.

The electricity dispatch results for the HIES with four MGs are shown in Fig. 11, including day-ahead scheduled and intraday real-time adjusted HIES net-load results and SOC results. The HIES net-load results are illustrated in Fig. 11 (a)–(d). The blue curves are the day-ahead scheduled HIES net-load profile, which will be used as the baseline for intraday actual operation. Yellow curves are the intraday actual operation net-load results, which are obtained in the intraday rolling dispatch stage and the intraday real-time adjustment stage. From the figures, the actual net-loads of four MGs are all close to the day-ahead results. Further, numerical results show that some deviations exist between day-ahead and real-time results due to the inevitable difference between day-ahead and short-term prediction. Day-ahead scheduled and intraday adjusted SOC results are illustrated in Fig. 11 (e)–(h) and (i)–(l), respectively. From Figs. 7, Figs. 10 and 11, the stored hydrogen, storage heat and the SOC results in day-ahead scheduling and intraday actual operation are slightly different. It suggests that the intraday rolling dispatch and the real-time adjustment model can effectively adjust the schedule results according to the latest demand variables. This flexibility allows for a more accurate and efficient allocation of resources, ensuring that the system operates optimally even in dynamic and uncertain operating conditions.

Further, to verify the economic performance of our proposed solution over a period, the Latin Hypercube sampling method [48] is used to sample scenes throughout a year and select 20 typical days. The sampling process involves three steps: (1) All scenes are evenly distributed in the interval [0,1], the interval is divided into 20 equal parts, and a random number is generated in each subinterval following a uniform distribution; (2) the order of 20 random numbers is scrambled to minimize the correlation of sampled each random variable; and (3) and the sample values are calculated using the inverse function of the probability distribution.

These selected days serve as test cases for assessing and comparing our proposed solution against three different benchmark solutions (benchmark 1, 2 and 3) described as follows.

Benchmark 1: energy management method proposed in Ref. [28].

Benchmark 2: the day-ahead schedule results of energy storage are executed without intraday corrections.

Benchmark 3: without hydrogen network, i.e. no hydrogen trading among MGs. MGs can only purchase hydrogen energy from the hydrogen market.

Fig. 12 shows the actual operation cost over test days for the HIES compared with benchmark 1 and benchmark 2 solutions. The proposed energy management solution and Benchmark 1 exhibit a mean actual operational cost of $3801.4 and $3843.3 respectively. On certain days, e.g., the 1st, 2nd, 4th, 9th, 12th and 13th day, Benchmark 2 outperforms the proposed method, indicating that both approaches effectively

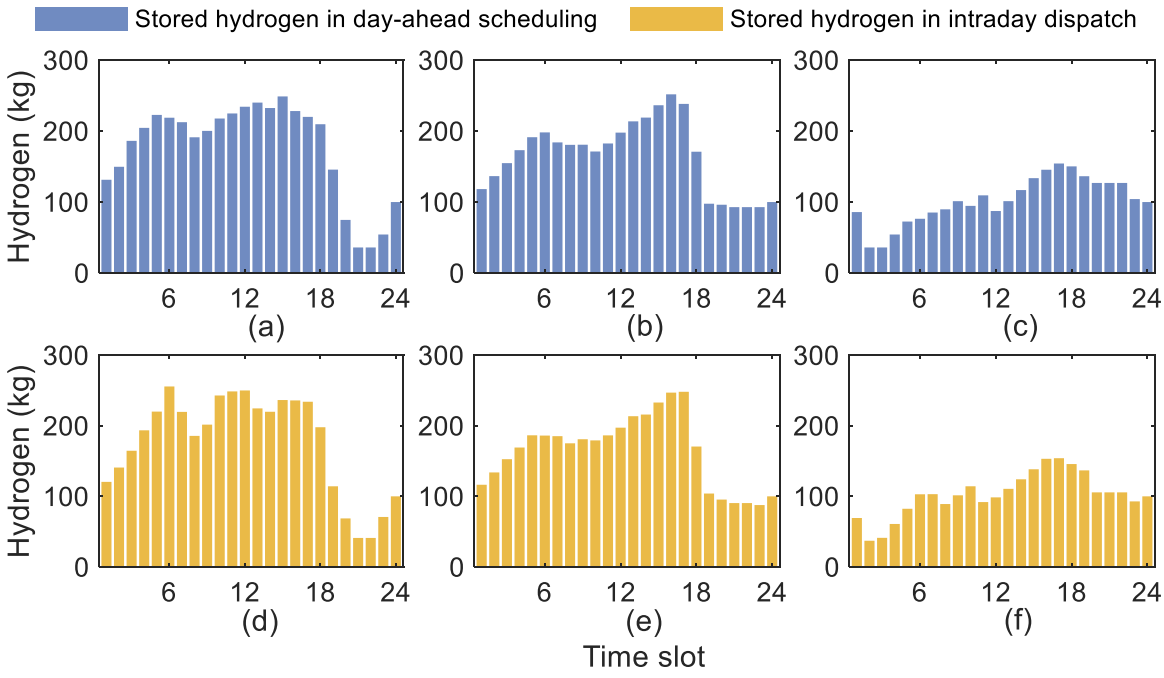

Fig. 7. Day-ahead scheduled and intraday real-time stared hydrogen results for (a) (d) EHI-CS1; (b) EHI-CS2; and (c) EHI-CS3.

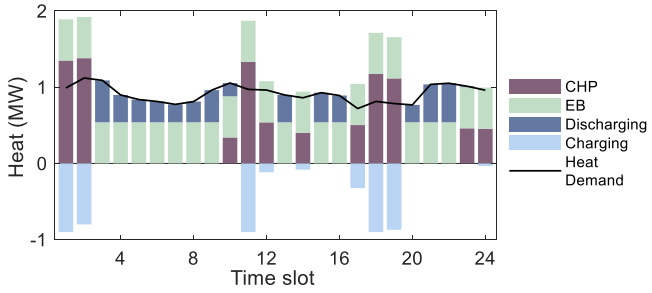

Fig. 8. HIES heat energy balance by the day-ahead scheduled for the industrial MG.

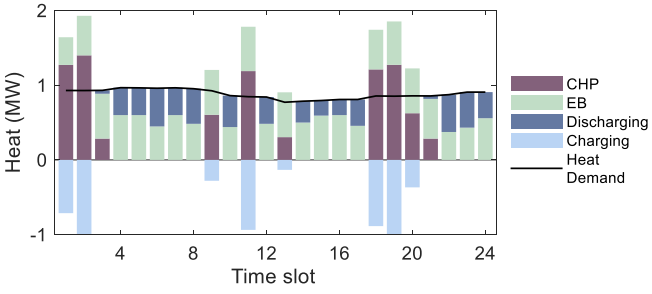

Fig. 9. HIES heat energy balance by the intraday real-time dispatch for the industrial MG.

address the energy management of the HIES. Moreover, the average execution time for making one-time slot decisions on electricity dispatch is 0.58s, significantly lower than Benchmark1's 3.37s. This reduction in computational complexity for real-time electricity dispatch can improve management efficiency.

In addition, the proposed solution exhibits a mean operational cost that is 25.56 % lower than Benchmark 2 ($4772.9). Notably, the proposed solution has a lower penalty cost in RTM than the benchmark2 solution over 20 test days. This demonstrates the effectiveness of intraday rolling dispatch and intraday real-time adjustments implemented in the proposed energy management solution, as they effectively mitigate the impact of prediction errors through the utilization of MPC-based rolling dispatch.

Further, Fig. 13 presents the actual operation cost over test days for the HIES compared with benchmark 3. The proposed solution demonstrates a significant reduction in mean operational costs, with a decrease of 6.91 % compared to Benchmark 2 (4772.9$). It can be found that the penalty cost resulting from participation in the RTM obtained with the proposed solution is larger than the benchmark3 on certain days, but the additional cost is smaller. This suggests that, in addition to dispatchable facilities, HIES includes an adjustment method of hydrogen trading among MGs that can flexibly coordinate day-ahead and real-time energy management.

4.3. *Further analysis for different hydrogen price*

Considering the development of hydrogen-based technologies and the dramatic growth in social hydrogen demand, the cost of hydrogen production and transportation is likely to significantly drop drastically, leading to a significant change in hydrogen prices in the future [40]. In this regard, three different hydrogen pricing scenarios, i.e., high, medium and low prices, are considered for further analysis and discussion, which are illustrated in Table 2.

Table 3 presents the energy management results for three different hydrogen price scenarios, including the hydrogen transaction value among MGs, hydrogen purchased from the hydrogen market, and the daily operational cost. It is evident that with decreasing hydrogen prices, the amount of hydrogen purchased from the hydrogen market increases, and the total operational cost of HIES decreases. This reduction in hydrogen costs makes it a more economically feasible and competitive energy alternative.

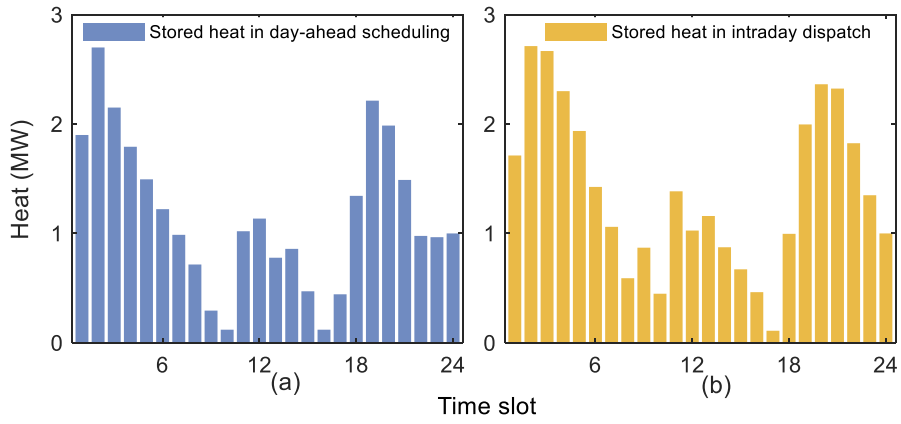

Fig. 10. Stored heat in industrial MG by (a) day-ahead scheduling result; and (b) intraday dispatch result.

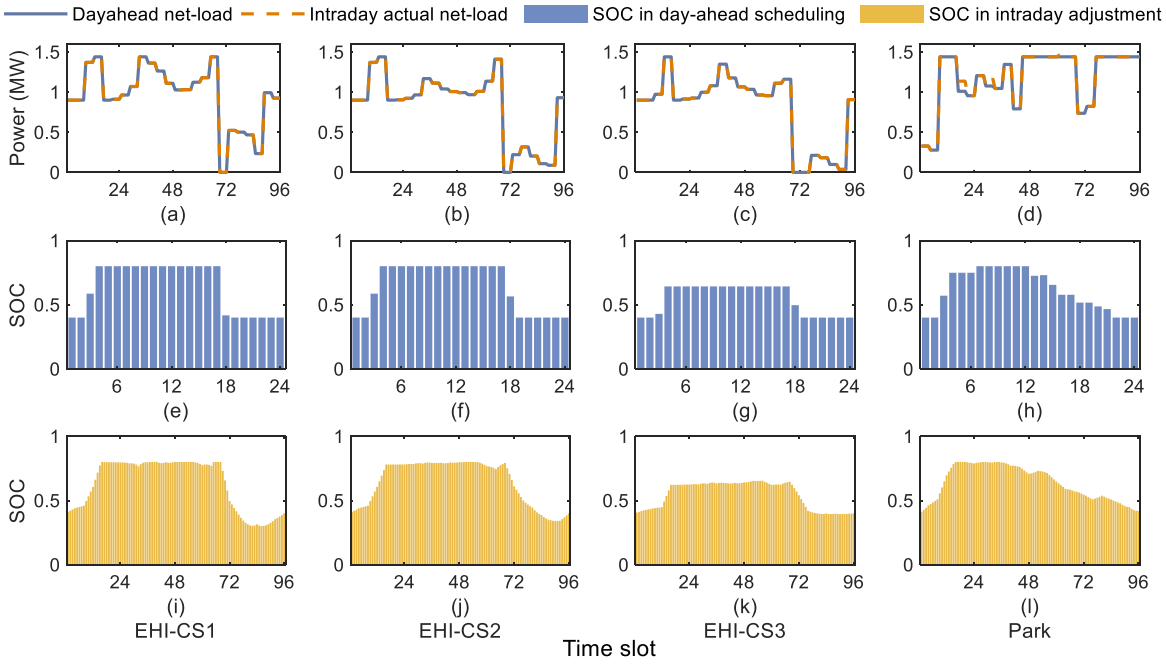

Fig. 11. Day-ahead scheduled and intraday real-time adjusted HIES net-load results and SOC results for (a) (e) (i) EHI-CS 1; (b) (f) (j) EHI-CS 2; (c) (g) (k) EHI-CS 3; and (d) (h) (l) industrial MG.

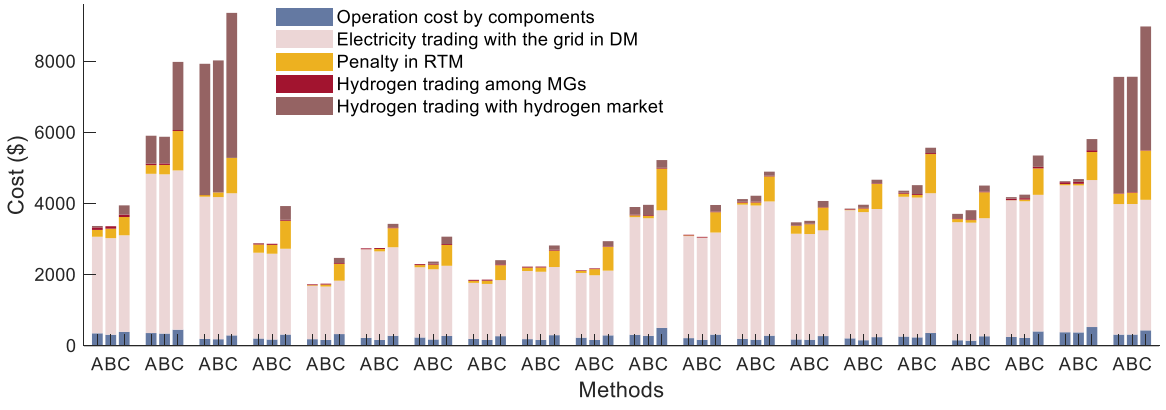

Fig. 12. Operational cost comparison over 20 test days. Note, A: proposed solution; B: benchmark 1 solution; and C: benchmark 2 solution.

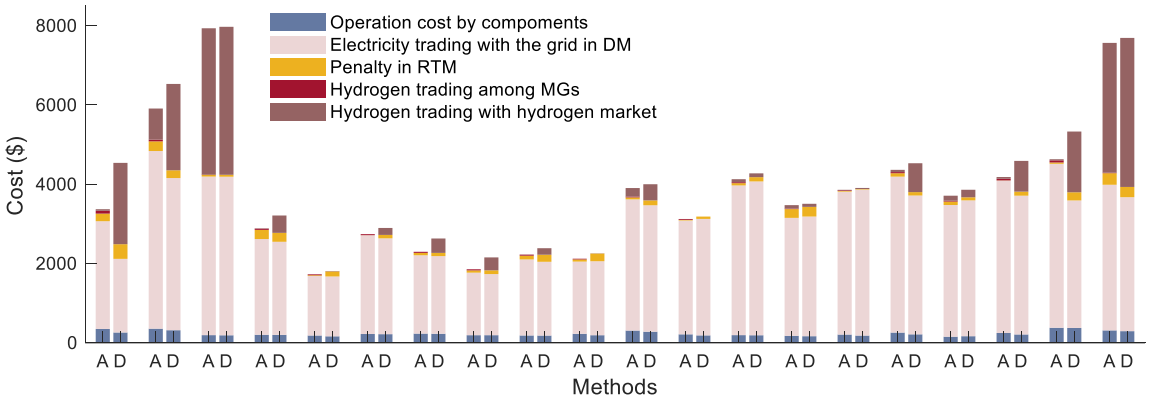

Fig. 13. Operational cost comparison over 20 test days. Note, A: proposed solution; and D: benchmark 3 solution.

Table 2
Different hydrogen price.

Hydrogen pricing Scenario	Hydrogen price of hydrogen market ($/kg)	Hydrogen selling price among MGs ($/kg)
High	6	3.6
Medium	4	2.4
Low	2	1.2

Table 3
Energy management results of three different hydrogen price scenarios.

Hydrogen pricing Scenario	Hydrogen transaction among MGs (kg)	Hydrogen purchased from hydrogen market (kg)	Daily operational cost ($)
High	466.69	25.87	7750
Medium	356.81	209.8	7584
Low	2.99	1643	5525

5. Conclusions

This paper presented a multi-stage and multi-timescale energy management solution for HIES with consideration of electricity-heat-hydrogen supply and demand balance and demand uncertainties. The coordination and tight couplings among multi-energy facilities and the hydrogen transaction among MGs are fully considered to enable the flexible HIES energy management and accommodate the electricity and hydrogen market. Moreover, the proposed solution for HIES is composed of three stages, including the day-ahead scheduling stage, intraday rolling dispatch stage and intraday real-time adjustment stage. The MPC-based strategy is utilized in the intraday rolling dispatch stage to reduce the impact of the demand uncertainties.

The proposed solution is assessed through simulation experiments using a 33-bus test network incorporating a HIES, and the numerical results demonstrate significant improvements. Due to the application of one-slot optimization in the intraday real-time adjustment stage, the computational complexity of electricity dispatch is reduced compared to benchmark 1. Moreover, the adoption of MPC in the intraday rolling dispatch stage can mitigate the impact of prediction errors, resulting in a significant reduction of 25.56 % in mean daily operational costs compared to benchmark 2. Further, the flexible management of energy within the HIES through the hydrogen trading method among MGs allows for effective adjustments. As a result, the actual operation cost decreases by 6.91 % when compared to Benchmark 3. These findings highlight the advantages and effectiveness of the proposed methods in terms of computational efficiency, economic performance, and overall system flexibility.

For future work, the following research directions are worthy of further exploitation: (1) Although the real-time electricity price and different constant hydrogen prices were considered, the dynamic pricing in the RTM is not studied. Thus, the dynamic hydrogen pricing schemes resulting from the RTM need to be considered in the energy management strategy for the HIES; and (2) The cost of the hydrogen investment can be offset by reducing the operating costs of the energy system. Therefore, the whole life-cycle cost-benefit analysis needs to be carried out for hydrogen energy utilization for the integrated energy systems.

Credit author statement

Xiaolun Fang: Conceptualization, Methodology, Data curation, Writing, Original draft preparation. Wei Dong: Investigation. Yubin Wang: Visualization. Yang Qiang: Supervision, Reviewing and Editing.

Declaration of competing interest

The authors declare that they have no known competing financial interests or personal relationships that could have appeared to influence the work reported in this paper.

Data availability

No data was used for the research described in the article.

Acknowledgments

This work is supported by the “Pioneer” and “Leading Goose” R&D Program of Zhejiang (2022C01239), the Special Support Plan for Zhejiang Province High-level Talents (2022R52012) and the National Natural Science Foundation of China (52177119).

References

[1] Nosratabadi SM, Hemmati R, Jahandide M. Eco-environmental planning of various energy storages within multi-energy microgrid by stochastic price-based programming inclusive of demand response paradigm. J Energy Storage 2021;36.
[2] Huang Y, Wang Y, Liu N. A two-stage energy management for heat-electricity integrated energy system considering dynamic pricing of Stackelberg game and operation strategy optimization. Energy 2022;244.
[3] Zhang C, Xu Y, Dong ZY. Robustly coordinated operation of a multi-energy microgrid in grid-connected and islanded modes under uncertainties. IEEE Trans Sustain Energy 2020;11:640–51.
[4] Yao T, Guan Y, Wang W. A high efficiency multi-module parallel RF inverter system for plasma induced hydrogen. Protection and Control of Modern Power Systems 2023;8(1):152–62.
[5] Banaei M, Rafiei M, Boudjadar J, Khooban M. A comparative analysis of optimal operation scenarios in hybrid emission-free ferry ships. IEEE Transactions on Transportation Electrification March 2020;6(1):318–33.
[6] Asensio FJ, San Martín JI, Zamora I, Garcia-Villalobos J. Fuel cell-based CHP system modeling using Artificial Neural Networks aimed at developing techno-economic efficiency maximization control systems. Energy 2017;123:585–93.

[7] Wang L, Jiao S, Xie Y, et al. " Two-way dynamic pricing mechanism of hydrogen filling stations in electric-hydrogen coupling system enhanced by blockchain ,". Energy 2022;239.
[8] Lahnaoui A, Wulf C, Heinrichs H, Dalmazzone D. Optimizing hydrogen transportation system for mobility by minimizing the cost of transportation via compressed gas truck in North Rhine-Westphalia. Appl Energy 2018;223:317–28.
[9] Mehrjerdi H. Off-grid solar powered charging station for electric and hydrogen vehicles including fuel cell and hydrogen storage. Int J Hydrogen Energy 2019;44 (23):11574–83.
[10] Thiel D. A pricing-based location model for deploying a hydrogen fueling station network. Int J Hydrogen Energy 2020;45(46):24174–89.
[11] Panah PG, Bornapour M, Hemmati R, Guerrero JM. Charging station stochastic programming for hydrogen/battery electric buses using multi-criteria crow search algorithm. Renew Sustain Energy Rev 2021;144.
[12] Khani H, El-Taweel NA, Farag HEZ. Supervisory scheduling of storage-based hydrogen fueling stations for transportation sector and distributed operating reserve in electricity markets. IEEE Trans Ind Inf 2020;16(3):1529–38.
[13] Qiu Y, Li Q, Ai Y, et al. Two-stage distributionally robust optimization-based coordinated scheduling of integrated energy system with electricity-hydrogen hybrid energy storage. Protection and Control of Modern Power Systems 2023;8 (2):542–55.
[14] Pan G, Gu W, Lu Y, Qiu H, Lu S, Yao S. Optimal planning for electricity-hydrogen integrated energy system considering power to hydrogen and heat and seasonal storage. IEEE Trans Sustain Energy 2020;11(4):2662–76.
[15] Fan G, Liu Z, Liu X, et al. " Two-layer collaborative optimization for a renewable energy system combining electricity storage, hydrogen storage, and heat storage,". Energy 2022;259.
[16] Mehrjerdi H, Hemmati R. Wind-hydrogen storage in distribution network expansion planning considering investment deferral and uncertainty. Sustain Energy Technol Assessments 2020;39.
[17] Ban M, Yu J, Shahidehpour M, Yao Y. Integration of power-to-hydrogen in day-ahead security-constrained unit commitment with high wind penetration. J Modern Power Syst Clean Energy 2017;5:337–49.
[18] Daneshvar M, Ivatloo BM, Zare K, Asadi S. Transactive energy management for optimal scheduling of interconnected microgrids with hydrogen energy storage. Int J Hydrogen Energy 2021;46(30):16267–78.
[19] Saatloo AM, Mirzaei MA, Ivatloo BM, Zare K. A risk-averse hybrid approach for optimal participation of power-to-hydrogen technology-based multi-energy microgrid in multi-energy markets. Sustain Cities Soc 2020;63.
[20] Herrmann A, Madlow A, Krause H. Key performance indicators evaluation of a domestic hydrogen fuel cell CHP. Int J Hydrogen Energy 2019;44:19061–6.
[21] Liu J, Xu Z, Wu J, Liu K, Guan X. Optimal planning of distributed hydrogen-based multi-energy systems. Appl Energy 2021;281.
[22] Liu J, Cao X, Xu Z, Guan X, Dong X, Wang C. Resilient operation of multi-energy industrial park based on integrated hydrogen-electricity-heat microgrids. Int J Hydrogen Energy 2021;46:28855–69.
[23] Saatloo AM, Ebadi R, Mirzaei MA, et al. Multi-objective IGDT-based scheduling of low-carbon multi-energy microgrids integrated with hydrogen refueling stations and electric vehicle parking lots. Sustain Cities Soc 2021;74.
[24] Wu Q, Xie Z, Ren H, Li Q, Yang Y. Optimal trading strategies for multi-energy microgrid cluster considering demand response under different trading modes: a comparison study. Energy 2022;254.
[25] Li P, Wang Z, Wang J, Guo T, Yin Y. A multi-time-space scale optimal operation strategy for a distributed integrated energy system. Appl Energy 2021;289.
[26] Zhong X, Zhong W, Liu Y. Optimal energy management for multi-energy multi-microgrid networks considering carbon emission limitations. Energy 2022;246.
[27] Liu H, Ma J. A review of models and methods for hydrogen supply chain system planning. CSEE Journal of Power and Energy Systems, early access 2020:1–12.
[28] Fang X, Dong W, Wang Y, Yang Q. Multiple time-scale energy management strategy for a hydrogen-based multi-energy microgrid. Appl Energy 2022;328: 120195.
[29] Zhou B, et al. Multi-microgrid energy management systems: architecture, communication, and scheduling strategies. J Modern Power Syst Clean Energy May 2021;9(3):463–76.
[30] Gaoa H, Liu J, Wang L, Liu Y. Cutting planes based relaxed optimal power flow in active distribution systems. Elec Power Syst Res 2017;143:272–80.
[31] Bao Z, Zhou Q, Yang Z, Yang Q, Xu L, Wu T. A multi time-scale and multi energy-type coordinated microgrid scheduling solution—Part I: model and methodology. IEEE Trans Power Syst 2015;30(5):2257–66.
[32] Liu Y, Zhang Y, Chen K, Chen SZ, Tang B. Equivalence of multi-time scale optimization for home energy management considering user discomfort preference. IEEE Trans Smart Grid 2017;8(4):1876–87.
[33] Garcia-Torres F, Bordons C. Optimal economical schedule of hydrogen-based microgrids with hybrid storage using model predictive control. IEEE Trans Ind Electron 2015;62(8):5195–207.
[34] Petrollese M, Valverde L, Cocco D, et al. Real-time integration of optimal generation scheduling with MPC for the energy management of a renewable hydrogen-based microgrid. Appl Energy 2016;166:96–106.
[35] Dong W, Yang Q, Li W, Zomaya AY. Machine-learning-based real-time economic dispatch in islanding microgrids in a cloud-edge computing environment. IEEE Internet Things J 2021;8(17):13703–11.
[36] Das S, Basu M. Day-ahead optimal bidding strategy of microgrid with demand response program considering uncertainties and outages of renewable energy resources. Energy 2020;190:1–13.
[37] Khani H, Farag HEZ. Optimal day-ahead scheduling of power-to-gas energy storage and gas load management in wholesale electricity and gas markets. IEEE Trans Sustain Energy Apr. 2018;9(2):940–51.
[38] Wang Y, Dong W, Yang Q. Multi-stage optimal energy management of multi-energy microgrid in deregulated electricity markets. Appl Energy 2022;310.
[39] ISO New England. Day-ahead hourly locational marginal price. http://www.iso-ne.com/isoexpress/web/reports/pricing/-/tree/lmps-da-hourly. [Accessed 10 February 2016].
[40] Bertuccioli L, Chan A, Hart D, et al. Development of water electrolysis in the European union. New Energy World 2014;31(1):140–7.
[41] Agency, U. S. Environmental protection. Catalog of CHP Technologies; 2014.
[42] Bao Z, Zhou Q, Yang Z, Yang Q, Xu L, Wu T. A multi time-scale and multi energy-type coordinated microgrid scheduling solution—Part II: optimization algorithm and case studies. IEEE Trans Power Syst 2015;30(5):2267–76.
[43] Wu X, Li H, Wang X, Zhao W. Cooperative operation for wind turbines and hydrogen fueling stations with on-site hydrogen production. IEEE Trans Sustain Energy 2020;11(4):2775–89.
[44] Sun S, Yang Q, Yan W. Hierarchical optimal planning approach for plug-in electric vehicle fast charging stations based on temporal-SoC charging demand characterisation. IET Gener Transm Distrib 2018;12:4388–95.
[45] Dong W, Yang Q, Li W, Zomaya AY. Machine learning based real-time economic dispatch in islanding microgrids in a cloud-edge computing environment. IEEE Internet Things J 2021;8(17):13703–11.
[46] Li R, Nahaei SS. Optimal operation of energy hubs integrated with electric vehicles, load management, combined heat and power unit and renewable energy sources. J Energy Storage 2022;48.
[47] Luo F, Ranzi G, Wan C, Xu Z, Dong ZY. A multistage home energy management system with residential photovoltaic penetration. IEEE Trans Ind Inf 2019;15(1): 116–26.
[48] Wyss GD, Jorgensen KH. *A user's guide to LHS: Sandia's Latin Hypercube Sampling Software*. States: N: United; 1998. https://doi.org/10.2172/573301.